Available online at www.sciencedirect.com
ScienceDirect
C. R. Physique 10 (2009) 116–129
COMPTES RENDUS PHYSIQUE

Laser acceleration of particles in plasmas / Accélération laser de particules dans les plasmas

Review of high-energy plasma wakefield experiments

Patric Muggli [a,*], Mark J. Hogan [b]

[a] *University of Southern California, Los Angeles, CA 90089, USA*
[b] *SLAC National Accelerator Laboratory, Menlo Park, CA 94025, USA*

Available online 29 April 2009

Abstract

Plasma wakefield accelerator (PWFA) experiments have made considerable progress in the past decade by using high-energy particle beams to drive large amplitude waves or wakes in a plasma. Electron beam driven experiments have measured the integrated and dynamic aspects of plasma focusing, the bright flux of high-energy betatron radiation photons, particle beam refraction at the plasma/neutral gas interface, and the structure and amplitude of the accelerating wakefield. Gradients spanning kT/m to MT/m for focusing and 100 MeV/m to 50 GeV/m for acceleration have been excited in plasmas with densities of 10^{14} to 10^{17} cm^{-3}, respectively. The large accelerating gradient led to the energy doubling of 42 GeV electrons in only 85 cm of plasma. Positron beam driven experiments have evidenced the comparatively more complex dynamic and integrated plasma focusing, the subsequent halo formation and emittance growth in the positron beam and demonstrated accelerating gradients of nearly 100 MeV/m. This article summarizes this experimental progress, illustrates the key enabling technologies that made the work possible, concludes with a brief discussion of proposed future directions, and suggests that the PWFA could one day revolutionize e^-/e^+ linear colliders. ***To cite this article: P. Muggli, M.J. Hogan, C. R. Physique 10 (2009).***

Résumé

Revue des expériences d'ondes de sillage excitées par faisceaux de particules de haute énergie. Les expériences d'ondes de sillage excitées par faisceaux de particules (PWFA en anglais) ont faits de remarquables progrès durant ces dix dernières années grâce à l'usage de faisceaux de particules de haute énergie pour exciter l'onde. Dans les expériences utilisant des faisceaux d'électrons, la dynamique de la focalisation du faisceau, le flux de photons produit par les oscillations bétatron, la réfraction des particules à l'interface entre le plasma et le gaz neutre, ainsi que la stucture et l'amplitude du champs accélérateur ont été mesurés. Des gradients de champs focalisatieurs du kT/m au MT/m, et des gradients accélérateurs de 100 MeV/m à 50 GeV/m on été excités dans des plasma avec des densités de 10^{14} à 10^{17} cm^{-3}, respectivement. La grande amplitude du gradient accélérateur a permis de doubler l'énergie des électrons de 42 GeV sur une longueur de seulement 85 cm de plasma. Les expériences avec des faisceaux de positrons ont mis en évidence le coté plus complexe de la dynamique de focalisation des positrons par le plasma, la formation d'un halo de charge autour du faisceau ainsi que la croissance de l'émittance du faisceau qui en découlent, et ont démontré l'excitation de gradients accélérateurs de presque 100 MeV/m. Cette revue résume ces progrès expérimentaux, illustre les technologies clés qui ont permis ces progrès, et se termine par une brève discussion des directions dans lesquelles ces recherches pourraient se diriger dans le futur. Elle suggère également qu'un jour le PWFA pourrait révolutioner le monde des accélérateurs linéaires e^-/e^+. ***Pour citer cet article : P. Muggli, M.J. Hogan, C. R. Physique 10 (2009).***

* Corresponding author.
E-mail address: muggli@usc.edu (P. Muggli).

1631-0705/$ – see front matter
doi:10.1016/j.crhy.2009.03.004

Keywords: Plasma-based accelerator; Plasma wakefield accelerator; Electron and positron acceleration; Electron and positron focusing; Betatron radiation

Mots-clés : Acceérateurs plasma ; Accélération d'électrons et de positrons ; Focalisation d'électrons et de positrons ; Radiation bétatron

1. Introduction

Plasma-based accelerators hold great promise to accelerate electrons, positrons, protons and ions to high energies over short distances and with high quality. They are one of the possible technologies that could revolutionize directly or indirectly many fields of science, medicine, and industry. The publication of this Special Issue is the evidence of this promise and of the intense research activity on these advanced accelerators. Plasma-based particle accelerators can, in principle, produce ultra-short, high charge and high current, low emittance and narrow energy spread beams. These beams will find applications for radiation generation for material and life sciences, electron microscopy, isotopes generation, cancer treatment, and high-energy physics. They may enable hospitals, research laboratories at universities, and industry, to afford devices that are currently only available at national laboratories and dedicated national or international facilities, such as light sources and accelerator complexes.

Plasma-based accelerators can be driven by laser pulses or by particle bunches. This article focuses on the particle beam-driven accelerator known as the plasma wakefield accelerator or PWFA [1], whose principle was first experimentally demonstrated in 1988 [2]. In particular, the recent spectacular progress in PWFA experiments at the Stanford Linear Accelerator Center (SLAC) is described and summarized. This progress was made possible by the unique properties of the electron beams available at SLAC: high energy (28.5 and 42 GeV) and charge ($\approx$3 nC), low normalized emittance ($<5\times10^{-5}$ m-rad) and ultra-short bunch length ($\approx$700 to $<$20 μm). Another unique feature of SLAC is the availability of positron bunches with parameters similar to those of electron bunches. This is particularly important for application of plasma-based accelerators to high-energy physics. In this context, plasma-based accelerators could one day allow for a significant reduction in the size [3] and cost of a future electron/positron linear collider. To reach this goal, the PWFA must be able to accelerate electron and positron bunches with a high accelerating gradient, to a high energy and with a narrow energy spread, while maintaining the incoming emittances. However, the plasma response to positron beams is not symmetric to its response to electron beams, at least in the nonlinear regime of their interaction. Therefore, research with both leptons is necessary and currently only possible at SLAC.

This article describes results of transverse dynamics and acceleration of electrons and positrons in plasmas for application to high-energy physics. These results include the first demonstration of the acceleration of positrons in plasmas [4], the matching of an electron beam to the plasma and the beam guiding over a 1.4 m-long PWFA module [5], the first demonstration of acceleration of electrons by more than 1 GeV in a plasma-based accelerator [6], as well as the *energy doubling* of 42 GeV incoming electrons in a plasma only 85 cm-long [7], i.e. with an accelerating gradient of $\approx$50 GeV/m. We also show that plasmas can be used as undulators to produce high-brightness beam of keV [8] to MeV [9] photons by betatron radiation. The very large accelerating gradients can also lead to trapping of plasma electrons [10] that can then be accelerated to multi-GeV energies and form low emittance, high peak current, ultra-short bunches [11]. Other experimental results and key diagnostics that were necessary for these experiments are also described, while many results and details are not mentioned. These results represent significant progress toward the development of an e^-/e^+ PWFA-based linear collider or *PWFA-LC*.

2. The Plasma Wakefield Accelerator

In the PWFA a particle bunch travels in a neutral plasma of electron density n_e (see Fig. 1 (a)). The space charge field of the bunch displaces the plasma electrons and drives a plasma wave or wake. The plasma wake oscillates at the electron plasma frequency ($f_{pe}=\omega_{pe}/2\pi$, $\omega_{pe}=(n_e e^2/\epsilon_0 m_e)^{1/2}$) and follows the drive bunch much the same way water wakes follow a fast boat. Its phase velocity is therefore equal to the drive beam velocity, and is independent of the plasma density. The wake has transverse focusing and defocusing, as well as longitudinal accelerating and decelerating fields. To the lowest order, the wake amplitude increases with the number of particles in the bunch N_b and the plasma density, and increases with decreasing bunch length σ_z and transverse dimension σ_r.

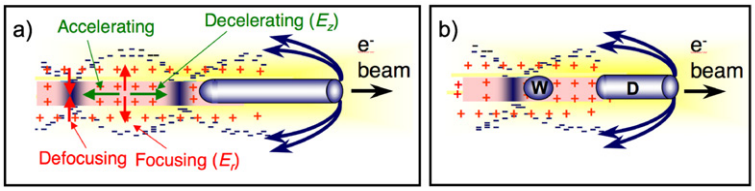

Fig. 1. Schematic of the plasma wakefield accelerator principle for (a) a single bunch, and (b) a drive (D), witness (W) bunch system. The wakefields are also cartooned in the second bucket of the wake in (a).

In practice, short particle bunches with dimensions of the order of the plasma wavelength $\lambda_{pe} = c/f_{pe}$ drive large amplitude plasma waves in high-density plasmas. The two-dimensional (2D) linear theory of the PWFA predicts that the maximum wake field amplitude that a single bunch can drive is given by [12,13]:

$$E_{acc}\ [\mathrm{MV/m}] = 244 \frac{N_b}{2\times 10^{10}} \left(\frac{600}{\sigma_z\ [\mu\mathrm{m}]} \right)^2 \tag{1}$$

This field is reached when the parameters are such that: $\sigma_z/\lambda_{pe} \cong (\sqrt{2}\pi)^{-1}$. It is also assumed that $\sigma_r/\lambda_{pe} \ll (2\pi)^{-1}$, i.e., the beam is smaller than the collisionless plasma skin depth c/ω_{pe} in its transverse dimension. The linear theory is valid only when the beam density is much smaller than the plasma density ($n_b = N_b/[(2\pi)^{3/2}\sigma_z\sigma_r^2] \ll n_e$), and the plasma density perturbation δn_e associated with the wake is small ($\delta n_e/n_e \ll 1$). With these conditions Eq. (1) can be rewritten as a function of the plasma density as:

$$E_{acc}\ [\mathrm{MV/m}] = 244 \frac{N_b}{2\times 10^{10}} \frac{n_e\ [\mathrm{cm}^{-3}]}{1.6\times 10^{14}} \tag{2}$$

Equations (1) and (2) show that a beam with $N_b = 2\times 10^{10}$ particles, $\sigma_z = 600$ μm, $\sigma_r \ll 600$ μm, accelerating gradients of the order of 200 MV/m can be driven in a plasma with a density of $\cong 1.6\times 10^{14}$ cm^{-3}. This gradient is comparable to the highest one that can be sustained in conventional rf accelerator cavities [14]. However, if the bunch is compressed to a much shorter length (≈20 μm) with the same number of particles, and the plasma density increased to $\cong 1.4\times 10^{17}$ cm^{-3}, gradients in excess of 100 GV/m can be reached. This example shows the potential of the PWFA accelerator as a high-gradient particle accelerator. However, the careful reader noticed that with the above parameters the condition $n_b/n_e \ll 1$ is not satisfied and a nonlinear theory is necessary.

In the absence of a complete nonlinear theory, numerical simulations are necessary tools to obtain the actual field amplitudes. It is, however, beyond the scope of this article to review simulation results, and numerical results will simply be quoted when appropriate. In the case of an electron bunch, simulations with the fully relativistic PIC code OSIRIS [15] confirm the trend indicated by the 2D linear theory, and with electron bunches the gradients are of the same order as those predicted by Eqs. (1) and (2). In this nonlinear or blowout regime [16] with $n_b/n_e \gg 1$, a pure ion column with ion density $n_i = n_e$ is left behind the head of the drive bunch. The ion column is a focusing element free of geometric aberration with a focusing strength of the order of kT/m at $n_e \cong 10^{14}$ cm^{-3} and MT/m at $\cong 10^{17}$ cm^{-3}. Due to these large field gradients the electron bunch can propagate with a small size for a very long distance (meters), much longer than the natural divergence distance in vacuum (or beta function) for a beam with normalized emittance ϵ_N given by $\beta = \gamma\sigma_r^2/\epsilon_N$. It is this combination of large accelerating gradient, strong focusing strength, and ultra-relativistic speed of the driver that allows for large energy gains. At the same time, the large focusing force gives rise to interesting transverse dynamics and to the possibility of using the plasma as a very compact *plasma undulator*. For example, the 28.5 GeV electrons entering the plasma at a radius of 10 μm oscillate with a period of 2.1 cm and a peak magnetic field of 81 T in an ion column of density 2.7×10^{17} cm^{-3}. We review the experimental results obtained with *long* ($\sigma_z \cong 700$ μm or $\cong 2$ ps) electron and positron bunches, as well as with the *short* ($\sigma_z \cong 20$ μm or $\cong 70$ fs) electron bunches that became available at SLAC in 2002.

3. Generic experimental setup

Different experiments require different experimental setup [5,17], although the main components remain similar, and are shown on Fig. 2. The general beam and plasma parameters for the long and short bunch experiments are given

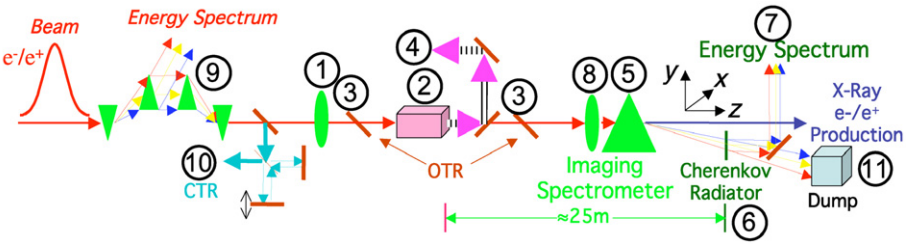

Fig. 2. Generic experimental set up for the PWFA experiments at SLAC. (1) Final beam focusing quadrupole doublet. (2) Plasma, in this case a Li vapor column, with variable density and length, produced in a heat-pipe oven. (3) OTR foils located ≈1 m upstream and downstream from the plasma entrance and exit, respectively. (4) Plasma light and beam diagnostic with wavelength resolution. (5) Energy spectrometer bending magnets. (6) Cherenkov radiator (aerogel). (7) CCD camera recording the visible Cherenkov light yielding the bunch energy spectrum after that plasma. (8) Magnetic quadrupoles imaging the beam at the plasma exit onto the Cherenkov radiator. (9) Weak vertical magnetic chicane where the beam dispersed in energy in the horizontal plane radiates synchrotron radiation, yielding the incoming bunch spectrum. (10) CTR diagnostic including bunch-to-bunch CTR energy measurement and CTR interferometry (multi-bunch). (11) Betatron x-ray diagnostics, including energy spectrum of e^-/e^+ pairs produced in a target.

Table 1
Typical parameters for the long and short bunch experiments.

Parameter/symbol/unit	Long bunch	Short bunch
Beam	e^- and e^+	e^-
Energy E_0 (GeV)	28.5	28.5, 42
Beam relativistic factor γ_0	55,773	55,773, 82,192
Bunch length σ_z (μm)	730	50 to 15
Bunch radius $\sigma_{x,y}$ (μm)	30, 30	10, 10
Bunch population N_b	$1.8 \times 10^{10} e^-$, $1.2 \times 10^{10} e^+$	1.8×10^{10}
Beam density n_b (cm^{-3})	1.8×10^{15}, 1.2×10^{15}	2.3×10^{17} to 7.6×10^{17}
Normalized emittance[a] $\epsilon_{Nx,y}$ (m-rad)	50, 5×10^{-6}	50, 5×10^{-6}
Lithium plasma	Photo-ionized	Field-ionized
Density range n_e (cm^{-3})	10^{12}–5×10^{14}	10^{16}–3×10^{17}
Length L_p (cm)	140	10, 20, 30, 60, 90, 120

[a] Before scattering through foils and pellicles.

in Table 1. Strong quadrupoles (1) focus the beam near the entrance of the plasma (2) to reach a transverse beam size smaller than the plasma collisionless skin depth c/ω_{pe}. The transverse shape and size of the beam are monitored by imaging the optical transition radiation (OTR) emitted by the beam when traversing thin (1–25 μm) metallic foils (3) placed ≈1 m upstream and downstream from the plasma entrance and exit, respectively. The typical resolution is ≈6–10 μm. The OTR light imaged onto CCD cameras is used to discriminate against bunches that enter the plasma with a transverse tilt (upstream), and to observe the effect of the plasma focusing force on the beam (downstream). The Cherenkov radiation emitted by the beam in the He buffer gas of the lithium source or the OTR and coherent transition radiation (CTR) emitted at a thin foil placed ≈50 cm from the plasma exit (4) is also collected and dispersed in wavelength. A bending magnet (5) disperses the particle beam in energy to reveal the energy change imparted by the plasma. For long bunch ($\sigma_z \cong 700$ μm) experiments, a measurement without plasma yields the incoming energy spectrum. The dispersed beam produces visible light in a Cherenkov radiator (6) such as aerogel or air. The visible Cherenkov light is imaged onto a CCD camera (7) for time integrated energy spectrum measurements or on a streak camera for time resolved energy spectrum measurements with bunches longer than a few picosecond. In order to unambiguously measure energy change, as opposed to transverse momentum imparted by the very strong plasma focusing force on a beam with a transverse tilt, quadrupoles magnets (8) image the beam at the plasma exit onto the Cherenkov radiator [6]. Alternatively, a two-screen method can be used when the energy spectrum of the beam is too wide for the magnetic imaging spectrometer [18].

For ultra short ($\sigma_z < 50$ μm, $\tau < 170$ fs) bunches produced by magnetic compression [19], the incoming bunch spectrum is recorded using the synchrotron radiation the beam emits in a soft vertical magnetic chicane (9) placed in a region of the beam line with horizontal magnetic dispersion (last compression stage) [20]. The synchrotron x-rays intercept a cerium doped yag scintillator screen producing visible light that is recorded by a CCD camera. Numerical

simulations of the compression process using the two-dimensional ($z - p_z$) code LiTrack [21] indicate that within a restricted range of accelerator parameters there is a unique correspondence between the incoming bunch energy spectrum, and its peak current and bunch length [22]. However, the bunch current profile retrieval algorithm is time consuming and performed off-line. Therefore, in the experiment, the relative bunch length is recorded on a shot-to-shot basis by measuring the CTR energy emitted by the beam when traversing a 1 μm thick Ti foil (10) located ≈10 m upstream from the plasma. Transition radiation has a very broad spectrum and becomes coherent for wavelengths longer than the bunch length ($\lambda \gg 2\pi\sigma_z$). The CTR energy is proportional to the square of the number of particles in the bunch N_b, and inversely proportional to σ_z (Gaussian bunch). The bunch charge (or N_b) is measured in the beamline before and after the plasma. The CTR also carries information about the bunch current profile that can in principle be retrieved by CTR interferometry [23]. CTR interferometry has a number of practical limitations: 1) the trace is always symmetric; 2) it requires 100–1000 consecutive bunches for the acquisition of a single trace; 3) it requires the accurate collection, transport and measurement of very broad spectrum radiation and therefore often yields filtered and inaccurate traces [24]. However, the combination of CTR energy, interferometric measurements and profile retrieval yields sufficient knowledge of the beam longitudinal parameters.

In addition, x-ray diagnostics (11) placed after the beam has been deflected by the magnetic spectrometer measure the radiation emitted by the bunch particles along the plasma. This radiation is also converted into e^-/e^+ pairs that are subsequently counted and analyzed in energy (see Section 7.2).

The plasma itself (2) is characterized off-line. Lithium (Li) has many attractive features as plasma for the PWFA: 1) its first electron ionization potential is relatively low (5.392 eV), and it is therefore easy to ionize; 2) its second and third electrons have relatively high ionization potentials (75.638 and 125.451 eV) and are difficult to ionize; 3) its low atomic number ($Z = 3$) leads to very small scattering even through long and dense plasmas. The Li vapor is produced in a heat-pipe oven [25,26]. It is confined to the hot region of the oven by a room temperature helium buffer gas (He, ionization potential 24.587 eV). The Li vapor density n_0 is controlled through the He pressure, and the vapor column length by the number of heating elements used. Typical numbers are: a He pressure of ≈200 mTorr, and a temperature of ≈700 °C for $n_0 \cong 1.8 \times 10^{15}$ cm^{-3} and ≈34 Torr and ≈1000 °C for $n_0 \cong 2.7 \times 10^{17}$ cm^{-3}.

The ionization cross section for photo-ionization of lithium is $\sigma_i \cong 1.8 \times 10^{-18}$ cm^{-2} for photons with energies between 5.4 and 9 eV [27], so that plasmas with density-length product of the order of $n_e L_p \cong 1/\sigma_i$ can be generated without significant longitudinal gradients caused by photon absorption. Photo-ionization is therefore appropriate for the long bunch experiments (see Table 1 and Section 5.1) that require plasmas with $n_e \cong 0$–2×10^{14} cm^{-3} and $L_p \cong 1.4$ m. The Li vapor is photo-ionized by a nanosecond Ultraviolet (UV) laser pulse ($\lambda = 193$ nm, $h\nu = 6.3$ eV) made parallel to the particle beam by reflection off a thin, 45° mirror (not shown on Fig. 2). The mirror is placed between the upstream OTR screen and the Li column entrance. The plasma density is varied by adjusting the laser pulse energy (single photon process). The maximum fractional ionization is about 15%. The laser beam is slightly focused along the Li vapor column to compensate the photon absorption and maintain a constant plasma density (±5%).

Short bunch experiments require higher density plasmas with $n_e \cong 0$–3×10^{17} cm^{-3} (see Table 1 and Section 5.2) with $n_e L_p$ up to 3.6×10^{19} cm^{-2}. Fortunately, when the bunch is compressed to $\sigma_z < 200$ μm, its space charge field exceeds the threshold for ionization of the first Li electron over a time scale faster than the bunch length σ_z/c: ≈6 GV/m [28]. Therefore, in addition to driving its own wake, a short bunch creates its own plasma by field-ionization [29]. This ionization process greatly simplifies the experimental setup and the plasma density n_e is equal to the Li vapor density n_0.

4. Transverse dynamics

Plasmas can exert an extremely large transverse force on particle beams. This force originates from the transverse component of the plasma wakefield, or equivalently from the partial neutralization of the beam charge by a plasma with displaced electrons. In the experiments described here, the beam dynamics associated with this force is inferred from measurements of the beam transverse size downstream of the plasma, as a function of the plasma density. In the blowout regime of the PWFA ($n_b/n_e \gg 1$), the transverse force the plasma exerts on an electron beam varies linearly with radius, and the transverse dynamics is linear and described by an envelope equation. Such focusing preserves the beam incoming emittance. In contrast, the dynamics of positron beams is nonlinear and complicated, and is described using numerical simulations. We discuss these two cases in this section.

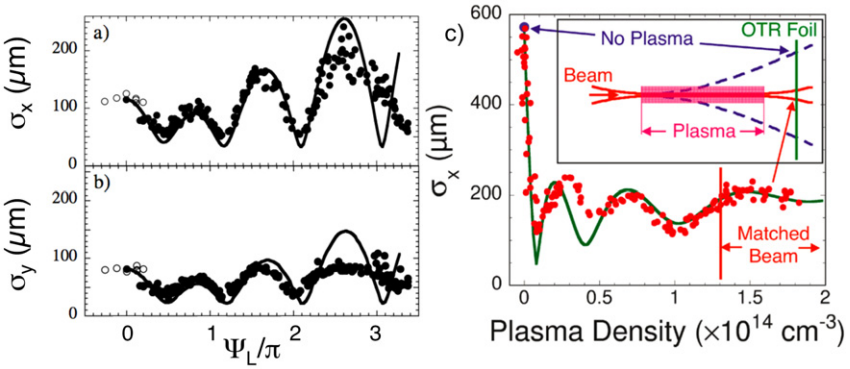

Fig. 3. Transverse electron beam sizes measured ≈1 m downstream from the plasma exit: (a) and (b) plotted as a function of the plasma phase advance $\Psi_L/\pi = \frac{1}{\pi}\int_0^{L_p}\frac{dl}{k_\beta} = \frac{L_p}{\lambda_\beta/2} \propto n_e^{1/2}L_p$, that is the number envelope betatron periods along the plasma [30]. (c) Plotted versus the plasma density [5]. The beam parameters are: (a) $\sigma_{x0} \cong 39$ μm, $\epsilon_{Nx0} \cong 8 \times 10^{-5}$ m-rad ($\beta_{x0} \cong 1.06$ m), (b) $\sigma_{y0} \cong 20$ μm, $\epsilon_{Ny0} \cong 3 \times 10^{-5}$ m-rad ($\beta_{y0} \cong 0.73$ m), and (c) $\sigma_{x0} \cong 30$ μm, $\epsilon_{Nx0} \cong 5.3 \times 10^{-4}$ m-rad ($\beta_{x0} \cong 0.11$ m). In (a) and (b) the waist is ≈50 cm upstream from the plasma entrance, in (c) it is at the plasma entrance. The inset of figure (c) shows schematically the beam envelope in vacuum (blue, dashed line) and in the matched beam case (red line). In all three case, the lines are the result of the envelope calculation (Eq. (3)) with the above parameters.

4.1. Transverse dynamics of electron beams in plasmas

In the nonlinear regime of the PWFA reached when $n_b/n_e \gg 1$ (and $k_p\sigma_r \ll 1$), the head of the drive bunch expels all the plasma electrons to a radius R of the order of the neutralization radius: $R \cong (n_b/n_e)^{1/2}\sigma_r$. The core of the drive bunch and a possible witness bunch therefore travel in a pure ion column of density $n_i = n_e$ (see Fig. 1) with a radial electric field $E_r = (n_e e/2\epsilon_0)r$. The ion column partially neutralizes the bunch charge, and acts as a strong focusing element free of geometric aberration since $E_r \propto r$, and E_r is constant along z. The focusing strength is $B_\theta/r = (E_r/rc)$, and reaches kT/m at $n_e \cong 10^{14}$ cm^{-3} and MT/m at $\cong 10^{17}$ cm^{-3}. Therefore, the beam electrons experience a harmonic oscillatory motion with wavelength $\lambda_\beta = 2\pi/k_\beta$, where $k_\beta = \omega_{pe}/(2\gamma)^{1/2}c$ and is deduced from the ion column electric field. When $\lambda_\beta \ll L_p$, the beam envelope experiences multiple betatron oscillations along the plasma with periodicity $\lambda_\beta/2$. On a screen placed downstream from the plasma exit these oscillations lead to variations of the beam transverse sizes as the plasma density is varied. They also lead to *betatron radiation*, as described in Section 7. Fig. 3 shows three examples of the beam transverse rms size measured approximately one meter downstream from the plasma exit [5,30] for 28.5 GeV, 700 μm-long electron bunches in plasmas with $n_e = 0$–1.8×10^{14} cm^{-3} and a length $L_p = 1.4$ m. As expected, all three figures exhibit oscillations with plasma density, corresponding to the various number of betatron periods of the beam envelope as a function of n_e. The beam envelope size $\sigma_{x,y}$ evolves along the pure ion column according to the envelope equation:

$$\sigma''_{x,y}(z) + \left(k_\beta^2(z) - \frac{\epsilon_{Nx,y}^2}{\gamma^2\sigma_{x,y}^4(z)}\right)\sigma_{x,y}(z) = 0 \tag{3}$$

where the plasma restoring term k_β is the same in the x and y directions, and may depend on the position along the plasma, either through the beam energy ($\gamma(z)$, energy loss or gain) or the plasma density $n_e(z)$. This equation can be integrated for the experimental beam and plasma conditions (including beam size and divergence at the plasma entrance) and then propagated ballistically ($k_\beta(z) = 0$) to the downstream screen. In the long bunch experiments discussed here, the electrons energy loss and gain (<300 MeV, see Section 5.1) is small compared to the beam energy (28.5 GeV), and therefore $\gamma \cong$ constant is used, and the plasma density is assumed to be constant over the plasma length. The results of the integration of Eq. (3) with the experimental parameters are also plotted on Fig. 3, and show good agreement with the measured results. The curves on Fig. 3 (a) and (b) have four minima, which indicates that at the highest density the beam has three foci inside the plasma. This is consistent with the ratio of the beam envelope betatron wavelength $\lambda_\beta = \pi/k_\beta$ to the plasma length L_p that is equal to three at the largest plasma density. Qualitatively, on Fig. 3 (a) and (b), the amplitude of the oscillation increases with n_e (or Ψ_L, see Fig. 3 caption), whereas it damps on Fig. 3 (c). This is due to the value of the term in parentheses in Eq. (3). It is larger than zero

for all values of $n_e \neq 0$ in Fig. 3 (a) and (b), which means that the beam is focused in the plasma to a transverse size smaller than the beam size at the plasma entrance. Therefore, as λ_β decreases with increasing n_e, the maximum divergence angle at the plasma exit ($\approx 4\sigma_{x,y}/\lambda_\beta \propto n_e^{1/2}$) also increases with n_e. On the contrary, in Fig. 3 (c) the beam parameters (σ_{x0}, ϵ_{Nx}) are such that the term in parentheses is smaller than zero a low n_e values, increases with n_e, and is equal to zero at

$$n_{e,m} = \frac{1}{2\pi r_e}\frac{\epsilon_N^2}{\gamma\sigma_{x0}^4} \cong 1.5 \times 10^{14}\ \mathrm{cm}^{-3}$$

where $r_e \cong 2.8 \times 10^{15}$ m is the classical electron radius, and σ_{x0} is the beam size at the plasma entrance. At this plasma density the ion column focusing force exactly balances the beam divergence due to its finite emittance, and assuming that the beam is focused at the plasma entrance ($\frac{\partial\sigma_x}{\partial z} = 0$), the beam is matched to the plasma focusing force. The beam size therefore remains equal to σ_{x0} along the plasma, and the beam divergence when exiting the plasma is a weak function of n_e, a condition desirable in future *PWFA-LC* stages. In the case of Fig. 3 (c) this also occurs at a density close to the optimum for acceleration (see Section 5.1), and the beam is guided (and electrons accelerated) with a constant transverse size over $L_p = 1.4$ m or 12 of its incoming beta functions ($\beta_{x0} \cong 0.11$ m). In practice, it takes a finite amount of time for the plasma electrons to blow-out and for the pure ion column to form. Therefore, the head of a single bunch or of the drive bunch do not experience the full ion column focusing force, and thus exhibit a lower number of betatron oscillations than those traveling in the pure ion column. The dynamic nature of the ion column formation for the head of the bunch has been measured in the experiments and reported in Ref. [31], Fig. 8. The deflection of the electron beam at the plasma boundary has also been observed for the first time in these experiments [32]. The bending angle of the beam core trajectory follows a refraction law similar to Snell's law for a light beam at a dielectric boundary [33].

4.2. Transverse dynamics of positron beams in plasmas

The transverse dynamics of positron beams in plasmas in the nonlinear regime ($n_b/n_e \gg 1$) is rather different from that of electron beams. The plasma electrons are attracted towards, and flow through the positron bunch rather than being expelled, and the plasma electron density along and across the positron bunch is not uniform. The resulting focusing force varies nonlinearly across the bunch (geometric aberrations), and is not constant along the bunch, leading to mixing of the positrons trajectories. Since the positron bunch can draw in plasma electrons from out to a skin-depth, the plasma electron density can be compressed to locally exceed the bunch density, and is a function of the history of the propagation of the bunch along the plasma. Therefore, no simple model exists to describe the effect of plasma focusing on the positron bunch, and numerical simulations must be used. Experimentally, time resolved focusing by a 1.4 m-long, low density plasmas (small density length product, $5.74 \times 10^{10}\ \mathrm{cm}^{-2}$) for which the positron bunch does not evolve significantly in its transverse dimension along the plasma has been measured [34]. The focusing of a positron bunch with similar parameters by a short gas jet plasma was also demonstrated [35].

Fig. 4 (a) shows the transverse size of the positron beam in the x and y plane measured as a function of n_e, with plasma parameters similar to those used the electron beam in Section 4.1, i.e. with density length products in the 7×10^{15} to $7 \times 10^{16}\ \mathrm{cm}^{-2}$, and much larger than in the previous paragraph. Unlike with the electron bunch, no evidence of betatron oscillations of the beam envelope along the plasma is visible. In this case, the nonlinear plasma focusing force completely phase-mixes the positrons trajectories, and as a result, the positron bunch develops a beam halo [36]. The propagation of the positron bunch along the plasma is simulated for the experimental parameters using the code QuickPIC [37]. The transverse beam sizes obtained in the simulations (Fig. 4 (a)) are in excellent agreement with those measured in the experiment. Simulations also show that, as expected, with these beam and plasma parameters the beam emittance grows along the plasma and with n_e. The beam rms emittance is calculated from the simulated beam phase space. Fig. 5 shows that with $n_e = 2 \times 10^{14}\ \mathrm{cm}^{-3}$ the emittance of five z slices and of the whole bunch quickly grows along the first few centimeters (small $n_e L_p$ product) of the plasma, especially in the low emittance y plane. After that initial jump the growth is smaller. In this case the total emittance grows by factors of 8 and 35 in the x and y plane, respectively. Figs. 4 and 5 show that the beam exiting the plasma is essentially round, i.e. has approximately the same transverse sizes and emittances in both planes, while the incoming emittances differ by a factor >4. Plasmas with larger $n_e L_p$ products lead to slightly larger beam size and emittance. This is due to

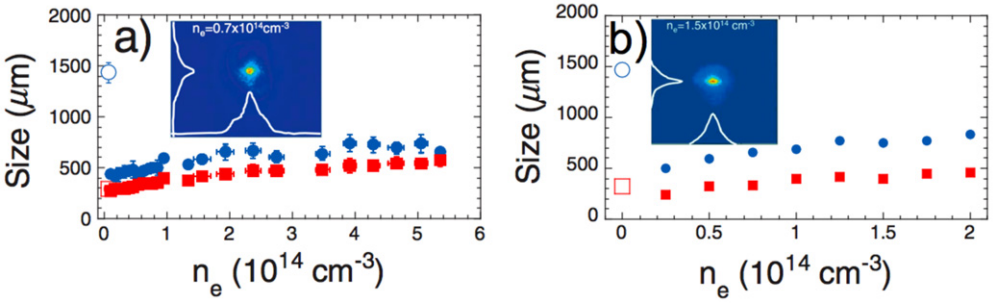

Fig. 4. (a) Transverse positron beam size in the x (blue symbols) and y direction (red symbols) measured ≈1 m downstream from the plasma exit as a function of the plasma density [36]. The empty symbols indicate the measurements without plasma ($n_e = 0$). The insert shows one of the beam image recorded with $n_e = 0.7 \times 10^{14}$ cm^{-3} together with the beam profiles (white lines). (b) Simulation results from the code QuickPIC for the beam transverse size at the same location and with the same beam parameters as in figure (a). The insert shows a simulated beam image with $n_e = 1.5 \times 10^{14}$ cm^{-3} together with the beam profiles (white lines). The agreement between the experimental results and the simulations is excellent. Bunch parameters: $\sigma_{x0} \cong \sigma_{y0} \cong 25$ μm, $\epsilon_{Nx} \cong 380 \times 10^{-6}$ m-rad, $\epsilon_{Ny} \cong 80 \times 10^{-6}$ m-rad.

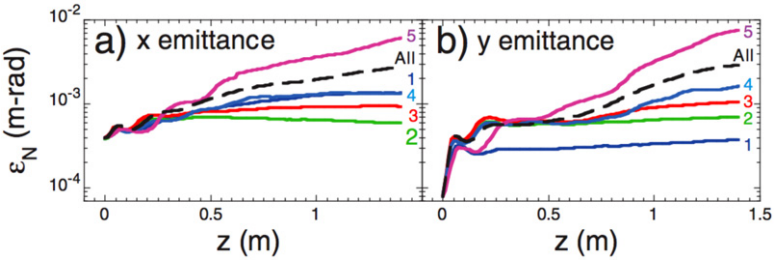

Fig. 5. Emittance of five z bunch slices (labeled from 1 in the front to 5 in the back) and of the whole beam (labeled *All*) in both the (a) x and (b) y plane, along the 1.4 m-long plasma [36]. The beam parameters are the same as those of Fig. 4.

the interplay between the beam and plasma densities that tends to equalize the beam parameters in the two different emittance planes.

The previous sub-sections show that the transverse dynamics of dense ($n_b > n_e$) electron and positron beams in meter-scale, dense plasmas is well understood. In the case of electron bunches, the focusing by the plasma pure ion column is free of geometrical aberration and preserves the incoming beam emittance. However, for future applications, chromatic aberrations resulting from the dependence of the plasma focusing force on energy $k_\beta = k_\beta(\gamma)$ in Eq. (3) require the acceleration of a narrow energy spread witness bunch. Positron bunches suffer emittance growth in uniform plasmas, and a means to preserve their incoming emittance must be devised. Propagation in a hollow plasma channel may minimize emittance growth, and at the same time increase the accelerating gradient driven by the positron bunch [38]. Transverse and longitudinal shaping of the witness bunch and operating a lower plasma density, i.e., with a more linear wake may also offer possible solutions for the preservation of the positron beam emittance.

5. Longitudinal dynamics, acceleration

The longitudinal component of the wakefield driven by a particle bunch in a plasma leads to energy loss by the particles in the front of a single bunch or in a short (compared to λ_{pe}) drive bunch. As the longitudinal wakefield reverses sign, particles in the back of the single bunch (Fig. 1 (a)), or in a trailing witness bunch (Fig. 1 (b)), can extract and gain energy from the wake. Presently, high energy experiments have only been performed with a single electron or positron bunch within the plasma wake. In such experiments, a single bunch fills all the phases of the periodic wakefield, which results in a large energy spread after interaction with the plasma. In this section we show that with electron bunches energy loss and gain are directly observed within a single long bunch, and that the energy gain scales inversely with the bunch length when the plasma density is adjusted as accordingly (see Section 2). The results presented here also show that the energy gain by trailing particles scales with the plasma length. These results

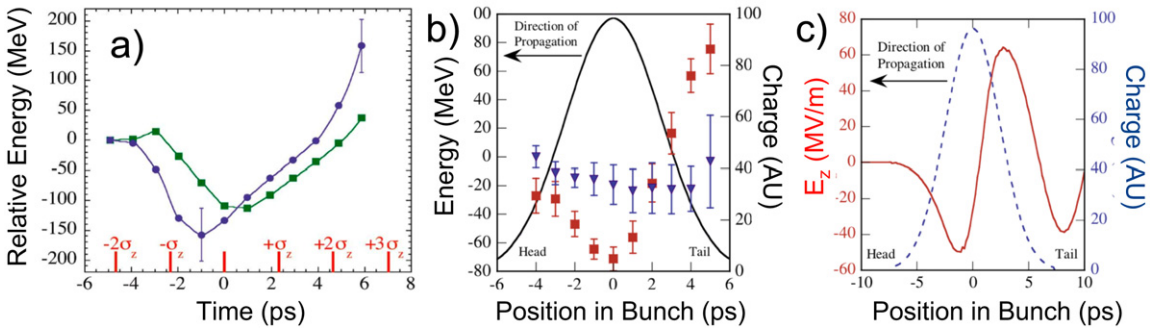

Fig. 6. (a) Time resolved relative energy of ≈1 ps-long electron bunch z slices for two different plasma densities: 1.5 (green squares) and 1.9 × 10^{14} cm^{-3} [5]. The maximum, slice-averaged energy gain is about 150 MeV. (b) Time resolved relative energy of ≈1 ps-long positron bunch z slices without plasma (blue triangles) and with $n_e = 1.8 \times 10^{14}$ cm^{-3} (red squares) [4]. (c) Simulated wakefield (red curve) driven by a positron bunch (blue curve) with the parameters of figure (b). The product of wakefield amplitudes and plasma length gives energy gain and loss numbers similar to those obtained from figure (b).

led to the demonstration of the energy doubling of 42 GeV electrons in only ≈85 cm of plasma, with an accelerating gradient of ≈50 GV/m. We also show that positrons can be accelerated in plasmas.

5.1. Acceleration of electrons

The first acceleration results with electrons are obtained with the long bunches ($\sigma_z \cong 700$ μm, see Table 1) in pre-ionized plasmas with densities in the 10^{14} cm^{-3} range (Eqs. (1) and (2)). Since the bunch is relatively long, and since ultra-relativistic particles do not dephase over meter distances, the energy of ≈1 ps-long z slices of the bunch can be measured with a streak camera. The imaging spectrometer is adjusted to image the beam at the plasma exit onto the aerogel radiator (see Fig. 2). The relative energy of each slice is plotted in Fig. 6. The energy change is obtained by subtracting the energy at large plasma densities from that measured at low density (0.7×10^{14} cm^{-3}) where the low density plasma guides the beam to the plasma exit without significantly changing its energy. The figure shows that the slices in the core of the bunch (≈0 ps) lose the maximum amount of energy. At the lower density (1.5×10^{14} cm^{-3}) the plasma wavelength is too long for the bunch length ($k_p\sigma_z < \sqrt{2}$), and while the wakefield reverses sign, no significant particles gain energy. At the higher density (1.8×10^{14} cm^{-3}) the plasma wavelength is short enough for the last measurable slice of the bunch to gain an average of ≈150 MeV over the $L_p = 1.4$ m plasma, corresponding to an average accelerating gradient of ≈100 MV/m [5]. However, careful analysis of the energy distribution in that slice reveals that some electrons gained ≈280 MeV, in an accelerating gradient of ≈200 MV/m. Note that for this combination of beam parameters and plasma density, the measured gradient is in agreement with Eqs. (1) and (2). This energy gain is obtained at the same time as the matching of the beam described in Section 4.1. While the gradient is not much larger than that envisioned for future accelerators [14], these results show the basic physics at play in a PWFA module.

Much shorter electron bunches can be produced by compression of the bunch in multiple stages [19], thereby taking advantage of the scaling of Eq. (1): $E_{acc} \propto N_b/\sigma_z^2$ with $N_b =$ constant, to produce much larger gradients (>10 GV/m) in higher density plasmas with bunches ≈20 μm long [24]. After the electron bunches are compressed their radial space charge field is large enough to field-ionize the Li vapor on the time scale of the bunch length. This self-ionization process greatly simplifies the experimental setup, and allows for the production of meter-scale plasmas with densities in the 10^{17} cm^{-3} range [29], which are extremely difficult to produce by photo-ionization. In order to keep the width of the final energy spectrum within the range of the imaging spectrometer (<20 GeV), the plasma length is reduced and made adjustable to 10, 20, and 30 cm. Fig. 7 shows the spectrum of the electron bunch without plasma (a), and after a 10 cm-long plasma with $n_e = 2.8 \times 10^{17}$ cm^{-3} (b). About 7% or ≈200 pC of the bunch charge gains energy, and the peak energy gain is ≈2.7 GeV [6] – the first energy gain exceeding 1 GeV in any plasma-based accelerator. With the plasma length extended to 30 cm, the maximum energy gain reaches 12.5 GeV, and scales linearly with plasma length [39]. In order to reach the largest energy gain, the beam energy is raised to 42 GeV, and the Li vapor column length extended to 85 cm. With the type of gradient expected from the previous measurements (>40 GV/m) the energy spectrum of the electron bunch after the plasma is expected to span from a few GeVs

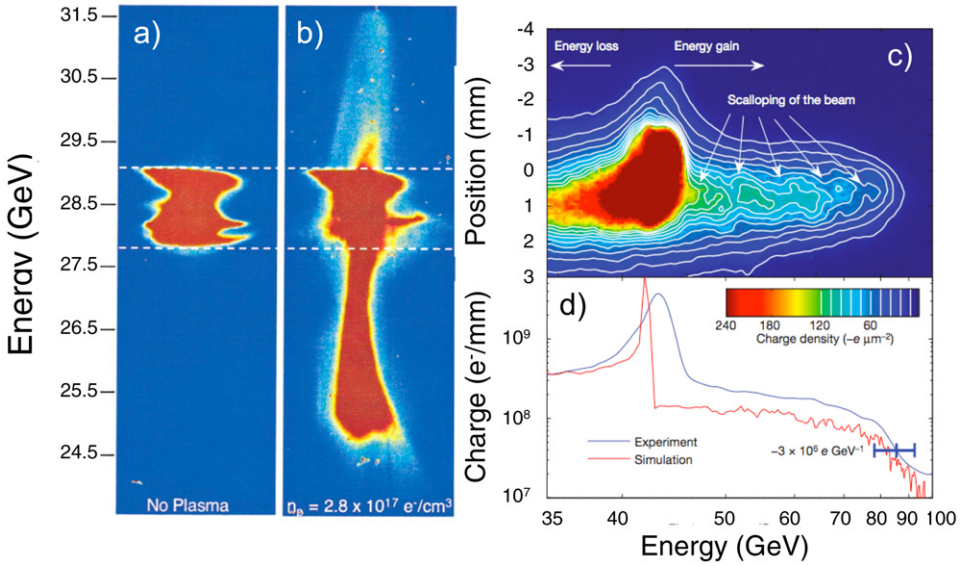

Fig. 7. Images of two identical incoming electron bunches $E_0 = 28.5$ GeV dispersed in energy along the vertical direction, measured (a) without plasma, and (b) after a 10 cm plasma with $n_e = 2.8 \times 10^{17}$ cm^{-3}. The peak energy gain reaches 2.7 GeV [6]. (c) Image of the 42 GeV beam dispersed in energy after the 85 cm plasma with $n_e = 2.8 \times 10^{17}$ cm^{-3}. The peak energy reaches 84 GeV, demonstrating the doubling of the energy of the bunch trailing particles [7]. (d) Energy spectrum obtained by summing the image of figure (c) along the non-dispersed axis (blue line), and obtained from numerical simulations using the code QuickPIC with the experimental parameters (red line).

to >75 GeV. Chromatic aberrations therefore dominate the transport along the beam line after the plasma, and the imaging spectrometer cannot be used. A simple bending magnet replaces the imaging spectrometer and a two-screen method is used to unambiguously differentiate between energy gain and transverse deflection [18]. Fig. 7 (c) shows that, with a $n_e = 2.7 \times 10^{17}$ cm^{-3} 85 cm-long plasma, some electrons reach 84 GeV gaining ≈42 GeV, corresponding to the doubling of their energy [7]. Fig. 7 (c) also shows that the bunch has energy left and that a larger energy gain in a longer plasma is possible. However, in these experiments the energy gain is limited by the erosion of the bunch head that propagates in the neutral Li vapor and expands as in vacuum. This leads to a continuous recess of the point along the bunch where the plasma is formed and of the point where the wake is generated. This effective loss of useful beam charge eventually terminates the ionization and wake excitation process [40]. However, this limit is not fundamental since it can be overcome by using a lower emittance beam. In this experiment the incoming beam suffers emittance growth through various foils that would not be present in a real accelerator.

5.2. Acceleration of positrons

The PWFA linear theory is symmetric for electron and positron bunches, therefore positrons can in principle also gain energy in a PWFA. This is demonstrated by Fig. 6 (b), which shows the time resolved slice energy measurement along a single positron bunch with and without plasma [4]. This figure is very similar to Fig. 6 (a) for an electron bunch with similar beam and plasma parameters. The energy gain and loss are less because the positron bunch has a lower number of particles ($N_b = 1.2 \times 10^{10}$) than the electron bunch ($N_b = 1.9 \times 10^{10}$), and because positrons tend to drive smaller amplitude wakes than electron bunches [38]. The measured energy gain and loss are also in good agreement with values of wakefield amplitudes obtained from simulations and multiplied by the plasma length L_p (Fig. 6 (c)).

6. Trapping of plasma electrons

In PWFA experiments with ultra relativistic beams the phase velocity of the plasma wake is equal to the beam velocity and is too large to trap plasma electrons that are born at rest either by photo- or field-ionization. However, in the experiments with ultra-short bunches described in Section 5.2, the total charge exiting the plasma is at times

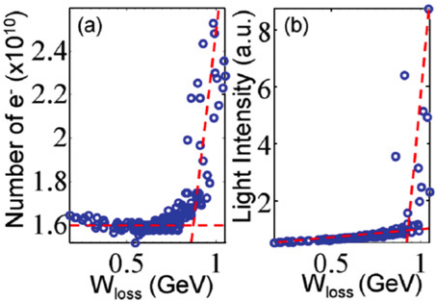

Fig. 8. (a) Number of electrons measured by a current transformer after the plasma as a function of the average beam electron energy loss over an $L_p = 10$ cm (FWHM), $n_e = 1.6 \times 10^{17}$ cm^{-3} [10]. The incoming beam population is constant at $\approx 1.6 \times 10^{10}$. (b) Cherenkov and OTR light amplitude produced by the beam collected after the plasma as a function of the average beam electron energy loss. Both curves show an excess in signal above an average energy loss of ≈ 0.9 GeV corresponding to a peak decelerating wake amplitude of ≈ 30 GV/m.

larger than the charge of the incoming electron beam, as shown by Fig. 8 (a). This occurs only when the average beam energy loss exceeds a threshold of 0.9 GeV/electron over ≈ 10 cm corresponding to a decelerating field amplitude of ≈ 30 GV/m [10]. This field amplitude is the threshold for trapping electrons born within the plasma wake. This trapping is made possible by the gas/vapor mixture in the Li heat-pipe oven. At the ends of the Li vapor column the He buffer gas and the Li vapor co-exist in the transitions regions. The low ionization potential Li is ionized first by the beam space charge field, but the higher ionization potential He is not. The Li plasma electrons sustain the plasma wake. As described in the previous sections, large wakefields are driven and the beam is focused. When the beam and wake transverse or longitudinal fields exceed the ionization field for He, He atoms are ionized inside the wakefield structure, and the new free electrons, born at rest, can be trapped [10]. These new electron are accelerated by the same wakefields that accelerate trailing bunch particles, have comparable energy gain and therefore reach multi-GeV energies [41]. Because of the small wakefield structure size, the trapped electrons also form ultra-short, low emittance bunches [11]. Fig. 8 (b) also shows a sudden jump in the amount of OTR and Cherenkov light collected immediately after the plasma and produced by the particles exiting the plasma. However, the relative amount of excess visible light is much larger that the relative amount of excess charge, indicating that some of the visible light is emitted coherently. Therefore a fraction of the trapped charge must have a time or bunch structure on the order of the coherent light period, or ≈ 1.7 fs for a typical $\lambda = 500$ nm. Spectral interferometry also reveals that more than one trapped bunch exits the plasma, and that the multiple bunches (two or three) are separated by approximately the plasma wavelength, indicated that, as expected, they are in subsequent wake buckets [42].

7. Betatron radiation

The behavior of the electron beam envelope in the plasma ion column was discussed in Section 4.1. The transverse size measurements confirm that the beam follows the envelope equation with a restoring term that can be derived from the ion column electric field. As the electrons oscillate in the ion column they emit synchrotron radiation often referred to as *betatron radiation*. Plasma-based accelerators operating in the blowout regime can therefore also be a source of x-ray radiation with a plasma undulator. The characteristics of the betatron radiation can be derived from standard synchrotron radiation theory. The frequency of the radiation is given by

$$\omega_{\beta r} = \frac{2n_h\gamma_0^2\omega_\beta}{1 + K^2/2 + (\gamma_0\theta)^2}$$

where n_h is the harmonic number, and θ is the observation angle measured from the beam axis and is assumed $\ll 1$. The plasma undulator strength is $K = \gamma_0\omega_\beta r_0/c$, where r_0 is the initial radial position of the electron when entering the plasma. Since each electron in the beam has a different r_0, the undulator strength and the radiation frequency are also continuous functions of r_0. Therefore the betatron radiation has a broad spectrum. Assuming the electrons do not lose much energy over a betatron period, either because of the wakefield or the radiation process ($\gamma(z) \cong \gamma_0$), the power radiated per betatron period can be written as $P_\beta \cong e^2\gamma_0^4 r_0^2\omega_\beta^4/3c^3$. Thus the radiated power scales as $\gamma_0^2 r_0^2 n_e^2$ ($\omega_\beta \propto n_e^2/\gamma^2$). The radiation is therefore dominated by that of electrons with large r_0 for which $K \gg 1$ (plasma

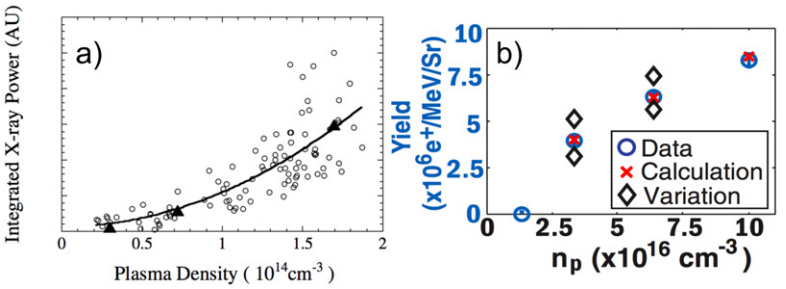

Fig. 9. (a) Measurement of the betatron yield in the energy range of 5–30 keV (empty circles) as a function of the plasma density. The triangles are the expected yields taking into account the experimental parameters [8]. The line is the quadratic fit to the experimental data $P_\beta \propto n_e^2$. Experimental parameters: $n_e = 1.7 \times 10^{14}$ cm^{-3}, $L_p = 1.4$ m, $r_0 = 40$ μm. (b) Yield of positrons with energies between 4 and 20 MeV measured and calculated as a function of plasma density [9]. The calculations include the energy loss by beam electrons, the actual beam radius in the plasma, and the number of beam electron inside the ion column. The black diamonds show the range calculated for $r_0 \pm 0.5$ μm.

undulator radiation). The broadband radiation has a critical frequency $\omega_c = 3\gamma_0^3 r_0 \omega_\beta^2/2c = 3K\gamma_0^2\omega_\beta/2$ (on axis) and lower frequencies are emitted within a cone angle given by $\theta_c = (\omega/\omega_c)^{1/3}/\gamma_0$.

7.1. Betatron radiation in low density plasmas

The optimum plasma density for acceleration with the long ($\sigma_z \cong 700$ μm) electron bunches is around 1.8×10^{14} cm^{-3} (see Section 5.1) and the plasma length is about 1.4 m. The critical frequency corresponds to photons with an energy of 111 keV, and the electrons undergo ≈1.6 betatron oscillations along the plasma (see Section 4.1). The maximum energy loss by the electrons is of the order of <300 MeV [5] and can be ignored for the synchrotron radiation measurements. Fig. 9 (a) shows that the $P_\beta \propto n_e^2$ is verified experimentally for the radiation in the 5–30 keV range, limited by the detector sensitivity [8]. The number of x-ray photons in a narrow energy range around 14.2 keV measured using Bragg reflection off a silicon crystal is $\approx 6 \times 10^5$. The corresponding peak spectral brightness is large: $\approx 7 \times 10^{18}$ photons/(s · mrad^2 · mm^2 · 0.1% bandwidth). Increasing the plasma density can increase the energy per photon, as well as their number.

7.2. Betatron radiation in high density plasmas

The short ($\sigma_z \cong 20$ μm) electron bunches experience large energy loss and gain, of the order of their incoming energy, in the $\approx 2.7 \times 10^{17}$ cm^{-3} plasma (Section 5.2). The betatron radiation spectrum is modified by this loss (most electrons lose energy), and the parameters for maximum betatron radiation may be different from those for maximum acceleration. In particular, if the betatron photons are to be converted to e^-/e^+ pairs, their energy must remain larger than $2m_e c^2 \approx 1$ MeV. With $n_e = 2.7 \times 10^{17}$ cm^{-3}, the critical photon energy is ≈50 MeV and decreases with γ^2. For plasma densities in the $3.3–10 \times 10^{16}$ cm^{-3} range, the betatron photon critical energy is lower and varies from 5.6 to 17 MeV. However, the vast majority of the photons have enough energy to create e^-/e^+ pairs. Therefore, the $P_\beta \cong \gamma_0^2 r_0^2 n_e^2$ should also apply to the number of positrons (or electrons) produced in a target. Fig. 9 (b) shows that, contrary to the case of Fig. 9 (a), the number of positrons resulting from pair creation and measured with energies between 4 and 20 MeV does not scale as n_e^2 [9]. This occurs because as n_e increases, the beam radius in the plasma decreases due to the focusing by the density ramp at the plasma entrance [43], the beam electrons lose more and more energy, and the number of beam electrons that are inside the fully formed plasma ion column also changes. Once these effects are taken into accounts, calculations of the positron yield follow the measured ones. This agreement confirms that the PWFA must be optimized as either an accelerator or as a plasma undulator.

The results presented in this section show that the PWFA can also be used as a radiation source to produce bright beams of x- and γ-rays. However, the beam and plasma parameters must be optimized either for radiation or for acceleration. Betatron radiation is unavoidable, but can be reduced by choosing a small beam radius ($P_\beta \propto r_0^2$). This will be a natural choice in future plasma-based accelerators operating with ultra-low emittance beams for which the radius matched to the plasma focusing force is also small. In this case, the energy loss to betatron radiation remains negligible when compared to the energy gain.

8. A look at the future

While the previous sections illustrate the tremendous progress made and the thorough understanding of the PWFA experiments, much remains to be done for the PWFA to reach a level where it could replace rf technology in a future e^-/e^+ linear collider. The acceleration of a trailing bunch instead of trailing particles is number one on the list. In a PWFA collider two accelerators will provide the drive and trailing bunch in trains appropriate for the collider design. The acceleration of a trailing bunch in a high-gradient PWFA has been demonstrated experimentally over a short distance [44]. Similar experiments proposed with the SLAC electron beam will use a mask technique [45] to split a single 25 GeV bunch into a drive and a trailing bunch. A short plasma section will then double the energy of the trailing bunch with a narrow relative energy spread (a few %). However, it is important to note that the acceleration of a trailing bunch with a narrow energy spread is *simply* a matter of producing the two bunches (for example, with two accelerators) and optimizing the acceleration process. With ultra-relativistic beams very little dephasing occurs between the particles accelerated and those decelerated over meter scale plasmas (the depletion length of the drive beam). For example, two particles with energies $E_2 \gg E_1 = 1$ GeV (maximum energy loss) dephase by only 0.7 μm ($\ll \sigma_z, \lambda_{pe}$) per meter of plasma length.

The same experiments need to be repeated with positron beams. However, in this case it is not clear yet whether the drive bunch will be an electron or a positron bunch. The masking technique applies equally well to positron bunches, however electron positron bunch pairs are not readily available. From an accelerator point of view it is more efficient to generate an electron drive bunch than a positron one. A new method to test the acceleration of positrons on the wake driven by electrons has been recently proposed [46]. This concept uses two electron bunches to produce the positron bunches in a thin target foil embedded in the plasma. The plasma transverse wakefield then selects the proper bunches. However, further numerical optimizations need to be carried out to test and optimize the acceleration of positron beams in plasmas.

Beyond these near term experiments, the preservation of the emittance of the incoming bunch (electron or positron) needs to be studied with beam with parameters similar to those required for a future collider.

The PWFA scheme needs to be integrated in a collider design that produces beams with parameters leading to the energy and luminosity required for future high-energy physics experiments. A luminosity in the 10^{34} cm^{-2} s^{-1} requires beams with average powers in the 10 MW range, posing new challenges for the drive beam production and the plasma generation. A careful optimization of the beam and plasma parameters is required to reach the maximum energy efficiency and minimize the accelerator cost. In particular, the number of plasma stages needs to be determined. A multi-stage accelerator will allow for a better control of the final beam parameters and for the mitigation of possible instabilities, such as the electron hose instability [47,48], through intermediate measurements and feedback systems. This is an endeavor that will require a sustained effort at the level currently invested in the design of future colliders [49]. However, the results summarized in this paper show that a single, 25 GeV stage of a plasma-based linear collider could be demonstrated very soon with the beam already available at SLAC (e^- and e^+). The PWFA accelerator is arguably the most advanced new accelerator concept that could one day revolutionize the world of high-energy e^-/e^+ colliders. In addition, many of the physics issues that can be addressed today in PWFA experiments (external injection, positron acceleration, beam quality preservation, etc.) are also relevant for the LWFA scheme, since the physics of the acceleration at high-gradient of a high-quality trailing bunch and the staging of accelerating structures are essentially independent of the wake driver and of the trailing beam injector. Therefore the systematic experimental study and development of all advanced accelerator concepts should be pursued to determine the best possible technique to reduce the size and cost of a future e^-/e^+ collider.

Acknowledgements

This work is supported in part by the US Department of Energy under contract Nos. DEFG03-92ER40745 and DE-AC02-76SF00515. The experimental and simulation results reported here were obtained by the collaborations E-157, E-162, E-164, and E-167 at the Stanford Linear Accelerator Center. We would like to thank all our collaborators as well as the SLAC technical and scientific staff without whom none of this would have been possible.

References

[1] P. Chen, et al., Phys. Rev. Lett. 54 (1985) 693.
[2] J.B. Rosenzweig, et al., Phys. Rev. Lett. 61 (1988) 98.
[3] S. Lee, et al., Phys. Rev. ST Accel. Beams 5 (2002) 121301.
[4] B.E. Blue, et al., Phys. Rev. Lett. 90 (2003) 214801.
[5] P. Muggli, et al., Phys. Rev. Lett. 93 (2004) 014802.
[6] M.J. Hogan, et al., Phys. Rev. Lett. 95 (2005) 054802.
[7] I. Blumenfeld, et al., Nature 445 (15 February 2007) 741–744.
[8] S. Wang, et al., Phys. Rev. Lett. 88 (2002) 135004.
[9] D.K. Johnson, et al., Phys. Rev. Lett. 97 (2006) 175003.
[10] E. Oz, et al., Phys. Rev. Lett. 98 (2007) 084801.
[11] N. Kirby, et al., in preparation.
[12] S. Lee, et al., Phys. Rev. E 61 (2000) 7014–7021.
[13] W. Lu, et al., Phys. Plasmas 12 (2005) 063101.
[14] H. Braun, et al., Phys. Rev. Lett. 90 (2003) 224801.
[15] R. Hemker, Ph.D. Thesis, UCLA (2000).
[16] J.B. Rosenzweig, et al., Phys. Rev. A 44 (1991) R6189.
[17] M.J. Hogan, et al., Phys. Plasmas 7 (2000) 2241.
[18] R. Ischebeck, et al., in: IEEE Particle Accelerator Conference, IEEE, Albuquerque, NM, 2007, p. 4168.
[19] P. Emma, et al., Stanford Linear Accelerator Center Report No. SLAC-PUB-8850, 2001 (unpublished).
[20] C.D. Barnes, Ph.D. dissertation, Stanford, 2005.
[21] K.L.F. Bane, P. Emma, in: IEEE Particle Accelerator Conference, IEEE, Knoxville, TN, 2005, p. 4266.
[22] I. Blumenfeld, et al., in preparation for Phys. Rev. Special Topics AB.
[23] C.J. Hirschmugl, et al., Phys. Rev. A 44 (1991) 1316.
[24] P. Muggli, et al., in: IEEE Particle Accelerator Conference, Knoxville, TN, 2005, p. 4102.
[25] C.R. Vidal, J. Cooper, J. Appl. Phys. 40 (8) (1969) 3370.
[26] P. Muggli, et al., IEEE Trans. Plasma Sci. 27 (1999) 791.
[27] G.V. Marr, Proc. Phys. Soc. 81 (1963) 9.
[28] M.V. Ammosov, N.B. Delone, V.P. Krainov, Sov. Phys. JETP 64 (1986) 1191.
[29] C.L. O'Connell, et al., Phys. Rev. ST Accel. Beams 9 (2006) 101301.
[30] C.E. Clayton, et al., Phys. Rev. Lett. 88 (2002) 154801.
[31] C.L. O'Connell, et al., Phys. Rev. ST Accel. Beams 5 (2002) 121301.
[32] P. Muggli, et al., Nature 411 (03 May 2001) 43.
[33] P. Muggli, et al., Phys. Rev. ST Accel. Beams 4 (2001) 091301.
[34] M.J. Hogan, et al., Phys. Rev. Lett. 90 (2003) 205002.
[35] J.S.T. Ng, et al., Phys. Rev. Lett. 87 (2001) 244801.
[36] P. Muggli, et al., Phys. Rev. Lett. 101 (2008) 055001.
[37] C. Huang, et al., J. Comp. Phys. 217 (2006) 658.
[38] S. Lee, et al., Phys. Rev. E 64 (2001) 045501.
[39] P. Muggli, et al., Proceedings PAC 07, 3076.
[40] M. Zhou, et al., in preparation and Ph.D. Thesis, UCLA, 2008.
[41] N. Kirby, et al., in: IEEE Particle Accelerator Conference, IEEE, Albuquerque, NM, 2007, p. 541.
[42] E. Oz, et al., in preparation for Phys. Plasmas.
[43] K.A. Marsh, et al., in: IEEE Particle Accelerator Conference, IEEE, Knoxville, TN, 2005, p. 2702.
[44] E. Kallos, et al., Phys. Rev. Lett. 100 (2008) 074802.
[45] P. Muggli, et al., Phys. Rev. Lett. 101 (2008) 054801.
[46] X. Wang, et al., Phys. Rev. Lett. 101 (2008) 124801.
[47] D.H. Whittum, et al., Phys. Rev. Lett. 67 (1991) 991.
[48] C. Huang, et al., Phys. Rev. Lett. 99 (2007) 255001.
[49] See for example: ILC Reference Design Report, August 2007, available at http://www.linearcollider.org/cms/?pid=1000025.